Acadlore Transactions on Applied Mathematics and Statistics
https://www.acadlore.com/journals/ATAMS

Simulation and Analysis of Torsional Vibrations in Carbon Fiber Sucker Rod Strings Induced by Helical Buckling Deformation

Xiurong Sun*, Chao Yu, Jialin Yang, Ruiju Zhao

Department of Environmental Engineering, Hebei University of Environmental Engineering, 066102 Qinhuangdao, China

* Correspondence: Xiurong Sun (sunxiurong@hebuee.edu.cn)

Received: 04-26-2025 **Revised:** 06-12-2025 **Accepted:** 06-24-2025

Citation: X. R. Sun, C. Yu, J. L. Yang, and R. J. Zhao, "Simulation and analysis of torsional vibrations in carbon fiber sucker rod strings induced by helical buckling deformation," *Acadlore Trans. Appl Math. Stat.*, vol. 3, no. 2, pp. 83–100, 2025. https://doi.org/10.56578/atams030201.

Abstract: To investigate the dynamic response and potential structural degradation of carbon fiber sucker rod strings during operation, a torsional vibration model incorporating helical buckling-induced torque excitation has been developed. In this model, the upper suspension boundary condition is idealized as a torsional spring, whose stiffness is determined as a function of both axial displacement and applied load at the suspension point. The torsional stiffness is categorized into time-dependent and mean (average) components, both of which are examined through numerical simulation using the finite difference method. The results reveal pronounced torsional oscillations at the upper section of the rod string, indicating significant torsional deformation of the suspension assembly. A non-monotonic relationship is observed between stroke length and vibration amplitude, wherein torsional vibration initially intensifies with increasing stroke before attenuating, suggesting the presence of resonance phenomena within specific operational ranges. The simulations further demonstrate that time-varying and average torsional stiffnesses yield comparable influences on the overall torsional response. Helical buckling deformation is shown to play a critical role in amplifying torsional stress, with the induced torque predominantly localized in the mid-to-lower segments of the wellbore. The presented model provides an essential theoretical framework for understanding the complex interaction between axial deformation and torsional instability, offering new insights into the mechanisms that may precipitate longitudinal splitting or fatigue failure in carbon fiber sucker rod strings. These findings are expected to support the optimization of rod string design and operational strategies in advanced artificial lift systems.

Keywords: Carbon fiber sucker rod; Helical buckling; Induced torque; Torsional vibration; Dynamic simulation; Resonance

1 Introduction

Carbon fiber sucker rods possess superior properties such as being lightweight, high- strength, and corrosion-resistant, making them suitable for deep, ultra-deep, and corrosive wells [1, 2]. The failure modes of carbon fiber sucker rods differ from those of steel sucker rods. According to the studied [3, 4], the primary failure modes of carbon fiber continuous sucker rods are disengagement and rod breakage, with the most common issues being splitting and broken wires, specifically transverse fractures and longitudinal splits. Among these, longitudinal split failure is unique to carbon fiber rods. Currently, the design methods for carbon fiber sucker rod strings are still based on simulations of axial vibration, axial load, and alternating axial stress, ensuring that carbon fiber rods do not experience compressive or axial stress and meet the API strength requirements, resulting in a combination of carbon fiber and steel heavy-duty rods [5]. Clearly, current designs for carbon fiber sucker rod strings focus solely on preventing transverse fractures in carbon fiber rods, without considering the strength conditions necessary for splitting. Transverse fractures are more likely to occur when subjected to alternating torque, alternating bending moment, or a combination of both. The phenomena such as the longitudinal splitting of the rod string, the twisting of the wire rope of the rope hanger and the helical scratch of the plunger of the oil well pump in the actual working process of the carbon fiber sucker rod string all indicate that the carbon fiber sucker rod string has torsional vibration [6, 7]. Therefore, establishing a torsional vibration simulation model for the carbon fiber sucker rod string

can enable quantitative analysis of these phenomena, which aids in exploring methods to prevent the damage of the carbon fiber sucker rod string from a theoretical perspective.

During the downward stroke, the carbon fiber sucker rod string experiences instability deformation due to axial pressure. As the axial pressure increases, the instability process begins with sinusoidal bending and then progresses to helical buckling [8–10]. The helical bending of the sucker rod string induces a torque [11–14], which changes periodically as the sucker rod bottom end bends under the forces from the reciprocating motion of the sucker pump's suspension point, thus exciting torsional vibrations in the sucker rod string. The studies [11, 12] suggest that the torsional vibration of the sucker rod string is caused by the torsion of the suspension rope and the torsional bending of the sucker rod. They define the upper boundary of the torsional vibration as the initial angle of rotation when the suspension rope experiences axial force, inducing a torsional torque, and the lower boundary as the concentrated effect of the torsional bending-induced torque on the plunger pair. They provide an analysis of the mechanism of the sucker rod string torsional vibration and a mechanical model. Zdvizhkov et al. [13] established a horizontal wellbore experimental platform. Using the experimental method, it was obtained that when the tubing reached the full helical shape, the internal torsion continued to increase with the increase of axial buckling force in the way of theoretical prediction, but the results were not given from the theoretical research. Chen et al. [14] established a mathematical model for the torsional vibration of the sucker rod string without considering damping, suggesting that analyzing the torsional state of the sucker rod can solve the torsional vibration of the sucker rod string, but no solution was provided. The studies [15, 16] investigated the torsional vibration of the rotating sucker rod string, but the rotating sucker rod string driven by surface-driven screw pumps produces continuous unidirectional active torque, while the torsional vibration of the rod pump sucker rod string system is mostly alternating or random effects, depending on the working conditions, thus there are significant differences between the two. Wang et al. [17] studied the torsional vibration of the sucker rod string under the influence of the curved wellbore trajectory in directional wells, which is significantly different from the study of the straight well sucker rod string torsional vibration in this paper. The studies [18–20] studied the buckling and post-buckling problems under torsional loads, exploring the influence of active torque on buckling, which has reference significance for this paper. However, it differs significantly from the research problem of induced torsional vibration caused by helical buckling in this paper.

The research by the aforementioned scholars provides a basis for analyzing the torsional vibration patterns of sucker rod strings. However, this paper suggests that the upper boundary should be the constrained angular displacement of the suspension device, the induced torque should be generated by the helical buckling segment, and the excitation torque should be the distributed torque applied to the helical buckling segment. Therefore, in this paper, the upper boundary of the suspension device in the mechanical model is simplified to a torsion spring, with the stiffness of the torsion spring varying with the displacement and load of the sucker pump's suspension point. The lower boundary is treated as a free end, and the helical buckling-induced torque is applied to the helical buckling segment as an excitation. A simulation model for the torsional vibration of carbon fiber sucker rod strings is established.

2 Methodology

The angular displacement of the top cross-section of the carbon fiber sucker rod is constrained by the suspension rope, so it is simplified as a torsion spring that responds to changes in the load and displacement at the pumping unit's suspension point. The bottom cross-section of the rod string, which is the plunger, is not constrained by the pump barrel, so it is simplified as a freely rotating end. For ease of study, the following assumptions are made:

(1) Assume that the well is a vertical well, and the sucker rod string and tubing are concentric;

(2) Taking the wellhead as the coordinate origin, periodic distributed torque is applied to the helical bending section of the rod string;

(3) The influence of coupling and centralizer on the local torsional stiffness of the rod string is not considered;

(4) The sucker rod string is a combination of two stages, and only the torsional vibration of the sucker rod string is considered.

Under the above assumptions, the torsional vibration dynamic model of the carbon fiber sucker rod string shown in Figure 1(a) is established. The force on the microelement at the section dx at the well depth x is shown in Figure 1(b).

In Figure 1, K_{e} is the torsional stiffness of the suspension rope; $G_1 J_{\mathrm{p1}}$ is the torsional stiffness of the carbon fiber rod; $G_2 J_{\mathrm{p2}}$ is the torsional stiffness of the steel rod; L_1 is the length of the carbon fiber rod; L_2 is the length of the steel rod; $M_{\mathrm{n}}(x,t)$ is the distributed torque subjected to periodic variation in the helical buckling section.

2.1 Suspension Load and Axial Distributed Load Simulation Model

The fluctuation equation is applied to describe the longitudinal vibration of the carbon fiber and steel hybrid sucker rod string, and the boundary condition and continuity condition are considered, so as to obtain the mathematical model of the longitudinal vibration of the hybrid rod string [21].

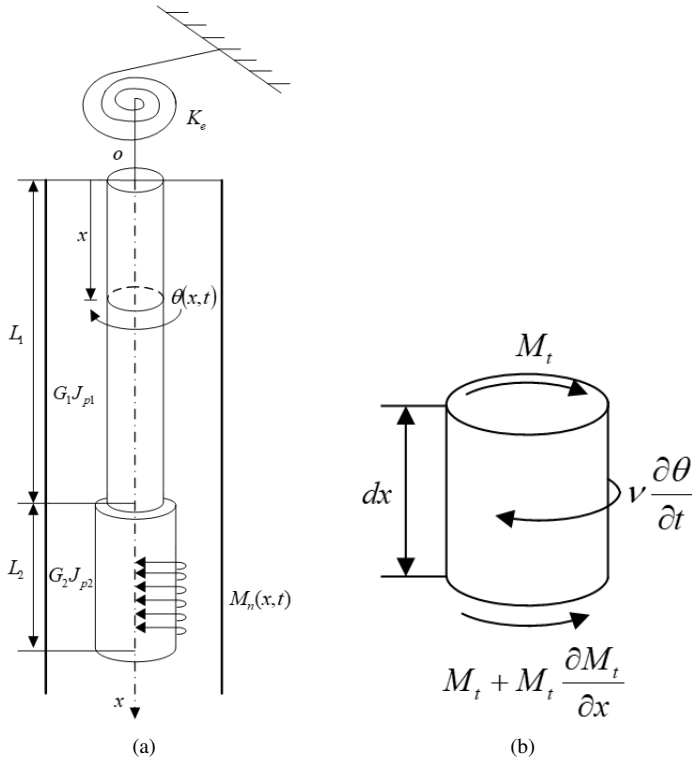

Figure 1. Twist vibration dynamic model of carbon fiber sucker rod string. (a) Rod mechanics model, and (b) force on a micro element

$$\begin{cases} \frac{\partial^2 u_1}{\partial t^2} - a_1\frac{\partial^2 u_1}{\partial x^2} + c_1\frac{\partial u_1}{\partial t} = -\frac{\partial^2 u^*(t)}{\partial t^2} - c_1\frac{\partial u^*(t)}{\partial t} \quad 0 \le x_1 \le L_1 \\ \frac{\partial^2 u_2}{\partial t^2} - a_2\frac{\partial^2 u_2}{\partial x^2} + c_2\frac{\partial u_2}{\partial t} = -\frac{\partial^2 u^*(t)}{\partial t^2} - c_2\frac{\partial u^*(t)}{\partial t} + \delta(x-L_2)F(t) \quad 0 \le x_2 \le L_2 \\ u_1|_{x_1=0} = 0 \\ E_2A_2\frac{\partial u_2}{\partial x_2}\Big|_{x_2=L_2} = 0 \\ u_1|_{x_1=L_1} = u_2|_{x_2=0} \\ E_1A_1\frac{\partial u_1}{\partial x_1}\Big|_{x_1=L_1} = E_2A_2\frac{\partial u_2}{\partial x_2}\Big|_{x_2=0} \end{cases} \tag{1}$$

In the formula, $u_1(x,t)$ represents the displacement of any cross-section x of the carbon fiber rod at time t relative to the suspension point, m; $u_2(x,t)$ represents the displacement of any cross-section x of the steel rod at time t relative to the suspension point, m; a_1 and a_2 are the propagation speeds of sound waves in the carbon fiber rod and the steel rod, $\mathrm{m/s}$, with $a_\mathrm{i} = \sqrt{E_i/\rho_i}$; c_1 and c_2 are the damping coefficients of the oil well fluid on the carbon fiber rod and steel rod, $1/\mathrm{s}$; A_1 and A_2 are the cross-sectional areas of the carbon fiber rod and steel rod, m^2; L_1 and L_2 are the lengths of the carbon fiber rod and steel rod, m; E_1 and E_2 are the elastic moduli of the carbon fiber rod and steel rod, Pa; ρ_1 and ρ_2 are the material densities of the carbon fiber rod and steel rod, $\mathrm{kg/m^3}$; $u^*(t)$ is the displacement of the suspension point, m; $F(t)$ is the axial load acting on the pump end, N.

The solution method of the suspension point displacement $u^*(t)$ and the pump end axial load $F(t)$ is given in detail by the study [18], which will not be repeated in this paper.

The difference method is applied to solve Eq. (1) to obtain $u_1(x,t)$ and $u_2(x,t)$. Considering the self-weight of the sucker rod string, the load of the pumping unit suspension point is calculated by the following formula:

$$P = W_r + \frac{E_1A_1}{\Delta x_1}\left(-\frac{3}{2}u_{0,j} + 2u_{1,j} - \frac{1}{2}u_{2,j}\right) \tag{2}$$

In the formula, W_r is the weight of the carbon fiber and steel sucker rod string, N.

The axial distributed load of the sucker rod string at any section x at time t is:

$$\begin{cases} q_1(x,t) = \frac{\partial\{\rho_2A_2gL_2+\rho_1A_1g(L_1-x)+E_1A_1[u_1(x+1,t)-u_1(x-1,t)]/(2\Delta x_1)\}}{\partial x} & 0 \le x \le L_1 \\ q_2(x,t) = \frac{\partial\{\rho_2A_2g(L_1+L_2-x)+E_2A_2[u_2(x+1,t)-u_2(x-1,t)]/(2\Delta x_2)\}}{\partial x} & L_1 < x \le L_1+L_2 \end{cases} \tag{3}$$

2.2 Torsional Stiffness Calculation Model

Figure 2 illustrates the schematic of a pumping unit suspension rope. The suspension rope consists of two steel wire ropes with opposite twists. If the suspension rope is subjected to a torsional moment T and rotates through an angle θ, as shown in Figure 3, the torque acting on the suspension rope can be divided into three components: the same- twist torsional moment T_{s}, the opposite-twist torsional moment T_{n}, and the swinging torsional moment T_{BT}, which can be expressed as:

$$\begin{cases} T = T_s + T_n + T_{BT} \\ T_s = \theta J_t G_s \\ T_n = \theta J_t G_n \\ T_{BT} = Ph \sin \beta / 2 \end{cases} \tag{4}$$

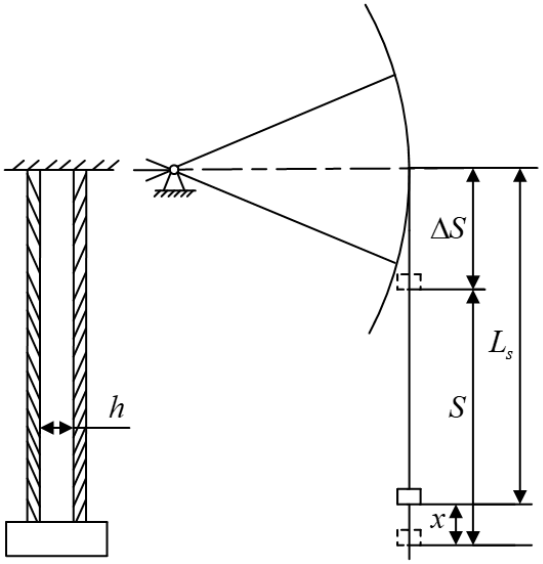

Figure 2. Schematic diagram of the suspension pulley

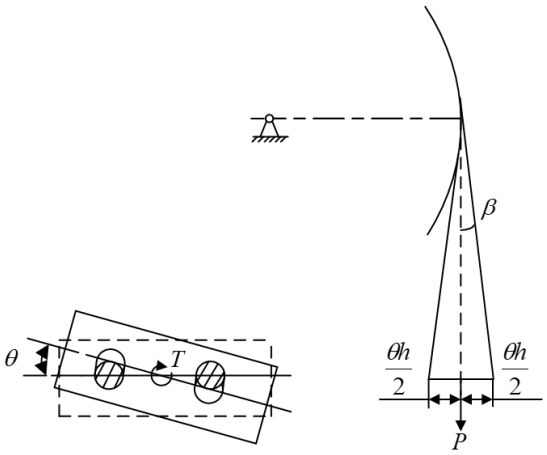

Figure 3. Force diagram of the suspension pulley

In the formula, J_t is the section modulus of the steel wire rope $J_t = \frac{\pi a^4}{32}$, m^4; a is the diameter of the steel wire rope, m; G_s is the shear modulus of the same-twist direction of the steel wire rope, in $\mathrm{N/m^2}$; G_n is the shear modulus of the opposite-twist direction of the steel wire rope, $\mathrm{N/m^2}$; P is the load on the suspension point, N; h is the distance between the two steel wire ropes, m; β is the angle between the steel wire rope and the vertical line, $\beta \approx \sin \beta = \frac{\theta h}{2L_s}$, $^\circ$; L is the length of the steel wire rope $L_s = S - x + \Delta S$, m; S is the stroke length, m; x is the suspension point displacement, m, and ΔS is the safety distance between the sucker rod string and the donkey head, m.

Write Eq. (4) in the form of $\frac{T}{\theta} = J_g G_g$, the torsional stiffness of the suspension device can be obtained in the form of $J_g G_g$.

2.3 Torsional Buckling Configuration and Induced Torque Calculation Model

The three-stage rod buckling mechanical model shown in Figure 4 is established: helical buckling bc section, spatial suspension Ab and cB section.

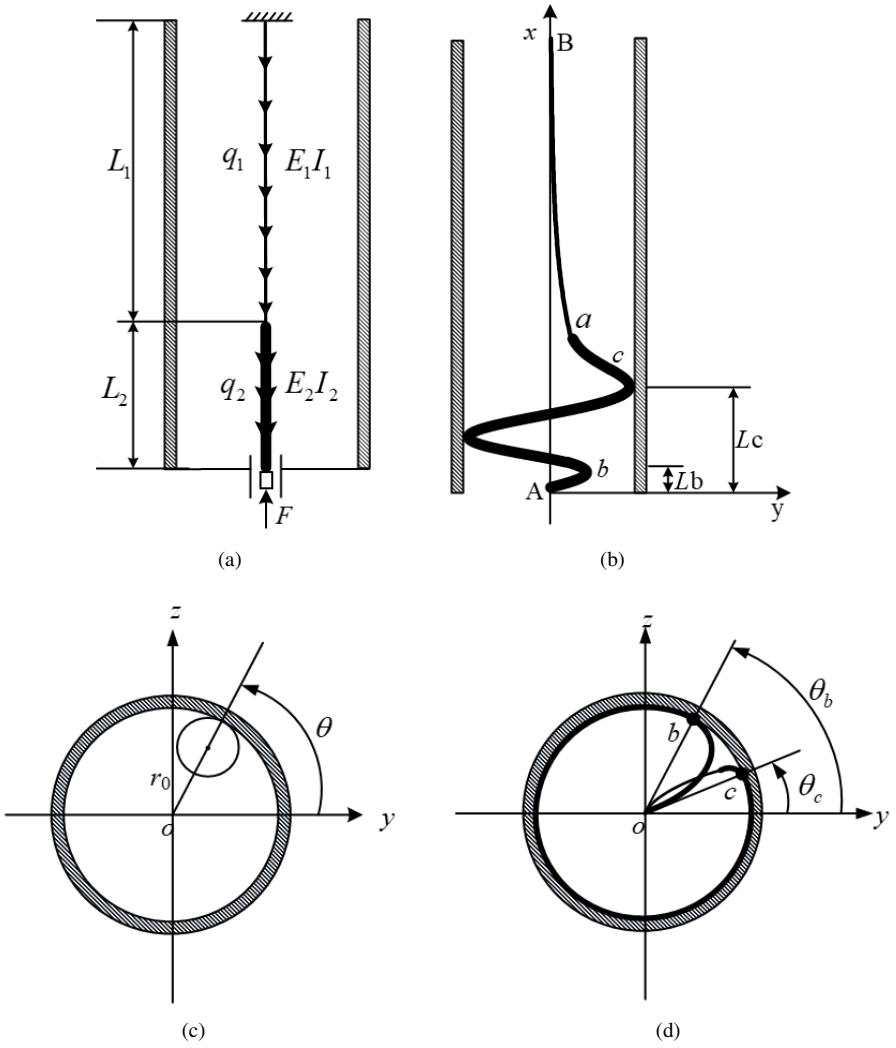

Figure 4. Mechanical model of three-stage bending configuration of sucker rod string. (a) Mechanics model, (b) sucker rod buckling configuration, (c) geometric position of the rod string, and (d) elevation view of rod string buckling

In the diagram, L_1 and L_2 represent the lengths of the carbon fiber rod and steel rod, m; q_1 and q_2 are the axial distributed loads on the carbon fiber rod and steel rod, respectively, $\mathrm{N/m}$; E_1I_1 and E_2I_2 are the bending stiffness of the carbon fiber rod and steel rod, respectively, $\mathrm{N \cdot m^2}$; F is the axial pressure at the bottom end of the sucker rod, N; a is the connection point between the carbon fiber rod and the steel rod; b and c are the contact points between the bottom suspension section and the upper suspension section with the tubing; L_b and L_c are the lengths from the bottom of the rod to the contact points with the tubing, m; θ represents the lateral deflection y and z at any axial position x along the suspension section in the Cartesian coordinate system, and the polar angle at any axial position x along the helical section in the polar coordinate system; θ_b and θ_c are the polar coordinates corresponding to the Cartesian coordinates b and c.

The differential equation of rod string helical buckling is:

$$E_2I_2\theta^{(4)} - 6E_2I_2\theta'^2\theta'' + \left[\left(F - \int_x^{L_1+L_2} q_2(x)dx\right)\theta'\right]' = 0 \quad L_b \le x \le L_c \tag{5}$$

The upper suspended section is a carbon fiber sucker rod string and a steel sucker rod string, and the bending equation is:

$$\begin{cases} E_1 I_1 \frac{d^4 y}{dx^4} + \frac{d}{dx}\left[\left(F - \int_0^{L_2} q_2(x)dx - \int_x^{L_1} q_1(x)dx\right)\frac{dy}{dx}\right] = 0 & 0 \le x \le L_1 \\ E_2 I_2 \frac{d^4 y}{dx^4} + \frac{d}{dx}\left[\left(F - \int_x^{L_1+L_2} q_2(x)dx\right)\frac{dy}{dx}\right] = 0 & L_1 \le x \le L_b \\ E_1 I_1 \frac{d^4 z}{dx^4} + \frac{d}{dx}\left[\left(F - \int_0^{L_2} q_2(x)dx - \int_x^{L_1} q_1(x)dx\right)\frac{dz}{dx}\right] = 0 & 0 \le x \le L_1 \\ E_2 I_2 \frac{d^4 z}{dx^4} + \frac{d}{dx}\left[\left(F - \int_x^{L_1+L_2} q_2(x)dx\right)\frac{dz}{dx}\right] = 0 & L_1 \le x \le L_b \\ \mathrm{y}_{x=L_1^-} = \mathrm{y}_{x=L_1^+} \quad \mathrm{z}_{x=L_1^-} = \mathrm{z}_{x=L_1^+} \frac{dy}{dx}\Big|_{x=L_1^-} = \frac{dy}{dx}\Big|_{x=L_1^+} \frac{dz}{dx}\Big|_{x=L_1^-} = \frac{dz}{dx}\Big|_{x=L_1^+} & \\ E_1 I_1 \frac{d^2 y}{dx^2}\Big|_{x=L_1^-} = E_2 I_2 \frac{d^2 y}{dx^2}\Big|_{x=L_1^+} E_1 I_1 \frac{d^2 z}{dx^2}\Big|_{x=L_1^-} = E_2 I_2 \frac{d^2 z}{dx^2}\Big|_{x=L_1^+} & \\ E_1 I_1 \frac{d^3 y}{dx^3}\Big|_{x=L_1^-} = E_2 I_2 \frac{d^3 y}{dx^3}\Big|_{x=L_1^+} E_1 I_1 \frac{d^3 z}{dx^3}\Big|_{x=L_1^-} = E_2 I_2 \frac{d^3 z}{dx^3}\Big|_{x=L_1^+} & \end{cases} \tag{6}$$

The bending equation of the bottom suspended section is:

$$\begin{cases} E_2 I_2 \frac{d^4 y}{dx^4} + \frac{d}{dx}\left[\left(F - \int_x^{L_1+L_2} q_2(x)dx\right)\frac{dy}{dx}\right] = 0 & L_c \le x \le L_1 + L_2 \\ E_2 I_2 \frac{d^4 z}{dx^4} + \frac{d}{dx}\left[\left(F - \int_x^{L_1+L_2} q_2(x)dx\right)\frac{dz}{dx}\right] = 0 & L_c \le x \le L_1 + L_2 \end{cases} \tag{7}$$

The boundary conditions are that both the top end of the rod and the pump end are fixed ends. Continuity conditions: the geometric, moment, and shear continuity conditions are satisfied at contact point b; the geometric, moment, and shear continuity conditions are satisfied at contact point c.

The numerical simulation process of the bending configuration is given in detail by the study [22]. From the above numerical simulation, the length of the spiral buckling section can be further calculated as follows:

$$L_d = L_c - L_b \tag{8}$$

In the study of rod buckling, a small unit is taken as the research object. Assuming the rod undergoes elastic deformation and the material is uniform across all segments, the rod can be considered a cylinder throughout the process. Based on these assumptions, the rod that exhibits helical buckling can be simplified into a cylindrical helix formed by an elastic line, as illustrated in Figure 5.

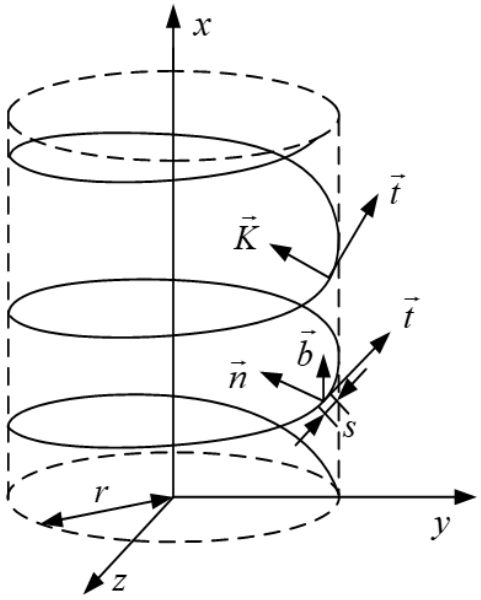

Figure 5. Mechanical analysis model of helical buckling rod string

In the figure, $\vec{K}$ represents the curvature vector of the simplified cylindrical helical space curve; $\vec{t}$ is the tangent vector of the cylindrical helical space curve; s denotes the arc length of any segment of the cylindrical helix, m; $\vec{n}$ is

the normal vector of the spatial curve; $\vec{b}$ is the secondary normal vector of the spatial curve; $\vec{u}$ is the spatial position vector; r is the radial clearance, m.

If M is the external torque in the rod string, then the equilibrium equation of torque is

$$\vec{M} = EI\kappa\vec{b} + M_n\vec{t} \tag{9}$$

In the formula, $EI\kappa\vec{b}$ is the bending moment in the rod string; κ is the curvature of the spatial curve; M_{n} is the torque in the rod string.

The cylindrical helical spatial curve has the following relationship:

$$\begin{cases} \vec{b} = \vec{t} \times \vec{n} \\ \vec{K} = \frac{d\vec{t}}{ds} = \kappa n \end{cases} \tag{10}$$

The tangent vector of a cylindrical helical space curve is

$$\vec{t} = \frac{d\vec{u}}{ds} = \left(\frac{dy}{ds}\right)\vec{i} + \left(\frac{dz}{ds}\right)\vec{j} + \left(\frac{dx}{ds}\right)\vec{k} \tag{11}$$

where, $\vec{i}, \vec{j}, \vec{k}$ respectively represent the unit vectors of the y, z, and x axis.

The curvature vector of the space curve is

$$\vec{K} = \frac{d\vec{t}}{ds} = \left(\frac{d^2y}{ds^2}\right)\vec{i} + \left(\frac{d^2z}{ds^2}\right)\vec{j} + \left(\frac{d^2x}{ds^2}\right)\vec{k} \tag{12}$$

The gap r between the rod and the tubing is very small compared to the helix formed by the rod, so it can be assumed that dz is three ds. Then we get

$$\vec{M} = \left(-EIz'' + M_n y'\right)\vec{i} + \left(-EIy'' + M_n z'\right)\vec{j} + \left(M_n + EI\left(y'z'' - z'y''\right)\right)\vec{k} \tag{13}$$

From the above formula, we can get the torque of each axis:

$$\begin{cases} M_y = -EIz'' + M_n y' \\ M_z = -EIy'' + M_n z' \\ M_x = M_n + EI\left(y'z'' - z'y''\right) \end{cases} \tag{14}$$

It can be obtained from Eq. (5):

$$\begin{cases} y = r\cos\theta & z = r\sin\theta \\ y' = -r\sin\theta\theta' & z' = r\cos\theta\theta' \\ y'' = -r\cos\theta\theta'^2 - r\sin\theta\theta'' \\ z'' = -r\sin\theta\theta'^2 + r\cos\theta\theta'' \end{cases} \tag{15}$$

Assuming there is no external torque on the x-axis, the internal torque of the rod string can be expressed as follows:

$$M_n(x,t) = E\,\mathrm{Ir}^2\,\theta'^3 \tag{16}$$

3 Mathematical Model of Twisting Vibration of Sucker Rod String

3.1 Equation of Torsional Vibration of Carbon Fiber and Steel Hybrid Rod String

The mathematical model of the torsional vibration of carbon fiber and steel hybrid rod string is obtained by micro-element force analysis:

$$\begin{cases} \rho_1 J_{p1}\frac{\partial^2\theta}{\partial t^2} + v_1\frac{\partial\theta}{\partial t} - G_1 J_{p1}\frac{\partial^2\theta}{\partial x^2} = 0 \quad 0 \le x \le L_1 \\ \rho_2 J_{p2}\frac{\partial^2\theta}{\partial t^2} + v_2\frac{\partial\theta}{\partial t} - G_2 J_{p2}\frac{\partial^2\theta}{\partial x^2} = \frac{\partial M_n(x,t)}{\partial x} \quad L_1 \le x \le L_1 + L_2 \\ G_1 J_{p1}\frac{\partial\theta}{\partial x}\Big|_{x=0} = K_e(t)\theta(0,t) \\ G_2 J_{p2}\frac{\partial\theta}{\partial x}\Big|_{x=L_1+L_2} = 0 \\ \theta|_{x=L_1^-} = \theta|_{x=L_1^+} \\ G_1 J_{p1}\frac{\partial\theta}{\partial x}\Big|_{x=x=L_1^-} = G_2 J_{p2}\frac{\partial\theta}{\partial x}\Big|_{x=x=L_1^+} \end{cases} \tag{17}$$

In the formula, ρ_1 and ρ_2 represent the densities of the carbon fiber rod and steel rod, $\mathrm{kg/m^3}$; ν_1 and v_2 are the resistance coefficients of the oil well fluid to the carbon fiber rod and steel rod, Pa.s; G_1 and G_2 are the shear moduli of the carbon fiber rod and steel rod, Pa; J_{p1} and J_{p2} are the polar moments of inertia of the cross-sections of the carbon fiber rod and steel rod, $\mathrm{m^4}$; $K_e(t)$ is the torsional spring stiffness derived from the simplified suspension device, $\mathrm{N \cdot m/rad}$; $M_n(x,t)$ is the distributed excitation torque, $\mathrm{N \cdot m}$.

3.2 Initial Condition

Assuming that the initial position of the carbon fiber and steel hybrid draw rod string is at the dead point under the suspension point and is in a natural stationary state, the initial condition of the whole system satisfying $t = t_0 = 0$ is:

$$\begin{cases} \theta(x,0) = 0 \\ \frac{\partial\theta(x,0)}{\partial t} = 0 \end{cases} \tag{18}$$

4 Vibration Torsion Simulation Method

The torsional spring stiffness varies with the displacement and load of the suspension point, making it time-varying. This paper first establishes a numerical simulation model for nonlinear vibration equations using the finite difference method, considering the time-varying torsional stiffness. To analyze the effect of stiffness on torsional vibration, we assume that the torsional stiffness is constant and take the average value of the torsional stiffness over one cycle. In this case, the torsional vibration is considered linear, and the mode superposition method is used for simulation and calculation.

4.1 The Difference Method Is Used to Establish the Simulation Model

The mathematical model for torsional vibration, which is a nonlinear differential equation, is used to describe the changes in torsional stiffness. The carbon fiber rod and steel rod are discretized into I_1 and I_2 units along the axis with unit lengths Δx_1 and Δx_2, respectively. The time t is discretized into $J+1$ nodes with a step length of Δt. $\theta_{i,j}\,(i = 0, 1, 2, \ldots, I_1, \ldots, I_1 + I_2)\,; j = 0, 1, 2, \ldots, J$ denotes the angular displacement of node i on the sucker rod string at time j.

Differential form of the differential equation at the carbon fiber rod:

$$\theta_{i,j+1} = \frac{1}{1+\gamma_{s1}}\left[\gamma_1\left(\theta_{i+1,j} + \theta_{i-1,j}\right) + 2\left(1-\gamma_1^2\right)\theta_{i,j} - \theta_{i,j-1} + \gamma_{s1}\theta_{i,j}\right] \tag{19}$$

In the formula, $\gamma_{s1} = v_1\Delta t; \gamma_1 = \sqrt{\frac{G_1}{\rho_1}}\frac{\Delta t}{\Delta x_1}$.

Differential form of the differential equation at the steel rod:

$$\theta_{i,j+1} = \frac{\varsigma}{1+\gamma_{s2}}\frac{\partial M_n(i,j)}{\partial x} + \frac{1}{1+\gamma_{s2}}\left[\gamma_2\left(\theta_{i+1,j} + \theta_{i-1,j}\right) + 2\left(1-\gamma_2^2\right)\theta_{i,j} - \theta_{i,j-1} + \gamma_{s2}\theta_{i,j}\right] \tag{20}$$

In the formula, $\varsigma = \frac{\Delta t^2}{\rho_2 J_{p2}}; \gamma_{s2} = v_2\Delta t; \gamma_2 = \sqrt{\frac{G_2}{\rho_2}\frac{\Delta t}{\Delta x_2}}$. The difference form of the differential equation at the connection point between the carbon fiber rod and the steel rod:

$$\theta_{i,j+1} = \frac{1}{\alpha_s + \beta_s}\left[\left(2\alpha_s + \beta_s - \mu_1 - \mu_2\right)\theta_{i,j} - \alpha_s\theta_{i,j-1} + \mu_1\theta_{i-1,j} + \mu_2\theta_{i+1,j}\right] \tag{21}$$

In the formula, $\alpha_s = \alpha_1 + \alpha_2; \beta_s = \beta_1 + \beta_2; \alpha_i = \frac{\Delta x_i (G_i J_{pi})}{2(c_i\Delta t)^2}, i = 1, 2; \beta_i = \frac{\Delta x_i (G_i J_{pi}) v_i}{2c_i^2\Delta t}, i = 1, 2;$ $\mu_i = \frac{G_i J_{pi}}{\Delta x_i}, i = 1, 2; \quad c_i = \sqrt{G_i/\rho_i}, i = 1, 2.$

The difference form of the upper boundary condition:

$$\theta_{0,j+1} = \frac{\frac{G_1 J_{p1}}{\Delta x_i}\left(3\theta_{1,j+1} - \theta_{2,j+1}\right)}{K_e(j+1) + \frac{2G_1 J_{p1}}{\Delta x_i}} \tag{22}$$

The difference form of the lower boundary condition:

$$\theta_{I_1+I_2,j+1} = \frac{G_2 J_{p2}\left(3\theta_{I_1+I_2-1,j+1} - \theta_{I_1+I_2-2,j+1}\right)}{2G_2 J_{p2}} \tag{23}$$

From the initial conditions, we know that $\theta(x,0) = 0$ and $\theta(x,1) = 0$. We discretize $\theta(x,0)$ and $\theta(x,1)$ along the axis.

The differential form of the differential equation, boundary condition, continuity condition, and initial condition established above constitute the simulation model of torsional vibration of carbon fiber sucker rod string.

4.2 The Superposition Method of Vibration Modes Is Used to Establish the Simulation Model

If the torsional spring stiffness K_e is taken as the average value of the torsional stiffness of a period, then the torsional vibration is linear vibration, so the super-position method of vibration modes is used to solve it.

4.2.1 Damping-free vibration equation of carbon fiber sucker rod string

The damping and induced torque in Eq. (17) can be removed to obtain the equation of free torsional vibration, whose solution is:

$$\begin{cases} \theta_1(x_1,t) = \Theta_1(x_1)F(t) = \left(C_1 \sin\frac{\omega}{a_1}x_1 + D_1\cos\frac{\omega}{a_1}x_1\right)(A_1\sin\omega t + B_1\cos\omega t) \\ \theta_2(x_2,t) = \Theta_2(x_2)F(t) = \left(C_2 \sin\frac{\omega}{a_2}x_2 + D_2\cos\frac{\omega}{a_2}x_2\right)(A_2\sin\omega t + B_2\cos\omega t) \end{cases} \tag{24}$$

In the formula, $\Theta_i(x)$ is referred to as the mode shape; ω represents the natural frequency of the torsional vibration of the carbon fiber sucker rod string. The eight undetermined coefficients can be determined through the boundary conditions, continuity conditions, and initial conditions. Substituting Eq. (24) into the boundary and continuity conditions yields the natural angular frequency equation and the mode shape function:

$$\mathrm{tg}\left(\frac{\omega}{a_1}L_1\right)\mathrm{tg}\left(\frac{\omega}{a_2}L_2\right) = \frac{G_1J_{p1}a_2}{G_2J_{p2}a_1} - \frac{G_1J_{p1}}{K_e}\frac{\omega}{a_1}\mathrm{tg}\left(\frac{\omega}{a_2}L_2\right) - \frac{G_1J_{p1}}{G_2J_{p2}}\frac{G_1J_{p1}}{K_e}\frac{a_2}{a_1}\frac{\omega}{a_1}\mathrm{tg}\left(\frac{\omega}{a_1}L_1\right) \tag{25}$$

$$\Theta(x) = \begin{cases} C_1\sin\frac{\omega}{a_1}x + D_1\cos\frac{\omega}{a_1}x & 0 \le x \le L_1 \\ C_2\sin\frac{\omega}{a_2}(x-L_1) + D_2\cos\frac{\omega}{a_2}(x-L_1) & L_1 \le x \le L_1+L_2 \end{cases} \tag{26}$$

In the formula, $C_1 = 1, D_1 = \frac{G_1J_{p1}\omega}{K_ea_1}, C_2 = \frac{G_1J_{p1}}{G_2J_{p2}}\left(\frac{a_2}{a_1}\cos\frac{\omega}{a_1}L_1 - \frac{G_1J_{p1}\omega a_2}{K_ea_1^2}\sin\frac{\omega}{a_1}L_1\right)$, $D_2 = \sin\frac{\omega}{a_1}L_1 + \frac{G_1J_{p1}}{K_ea_1}\cos\frac{\omega}{a_1}L_1$.

4.2.2 Regular mode

The orthogonality of the moment of inertia with respect to the main vibration mode can be obtained:

$$Y_r(x) = A_r\Theta(x) = \begin{cases} A_r\left(\sin\frac{\omega_r}{a_1}x + D_1\cos\frac{\omega_r}{a_1}x\right) & 0 \le x \le L_1 \\ A_r\left[C_2\sin\frac{\omega_r}{a_2}(x-L_1) + D_2\cos\frac{\omega_r}{a_2}(x-L_1)\right] & L_1 \le x \le L_1+L_2 \end{cases} \quad r = 1,2,\cdots \tag{27}$$

In which A_r is the regularization coefficient:

$$A_r = \sqrt{\frac{1}{\begin{array}{c}\rho_1J_{p1}\left(\begin{array}{c}\frac{L_1}{2} - \frac{a_1}{4\omega_r}\sin\frac{2\omega_r}{a_1}L_1 + \frac{a_1D_1}{2\omega_r} - \frac{a_1D_1}{2\omega_r}\cos\frac{2\omega_r}{a_1}L \\ + \frac{D_1^2L_1}{2} + \frac{D_1^2a_1}{4\omega_r}\sin\frac{2\omega_r}{a_1}L_1\end{array}\right) \\ + \rho_2J_{p2}\left(\begin{array}{c}\frac{a_2C_2D_2}{2\omega_r} + \frac{L_2}{2}\left(C_2^2+D_2^2\right) - \frac{C_2^2a_2}{4\omega_r}\sin\frac{2\omega_r}{a_2}L_2 \\ + \frac{D_2^2a_2}{4\omega_r}\sin\frac{2\omega_r}{a_2}L_2 - \frac{a_2C_2D_2}{2\omega_r}\cos\frac{2\omega_r}{a_2}L_2\end{array}\right)\end{array}}} \tag{}$$

4.2.3 Regular force and regular damping

When the carbon fiber sucker rod string is excited by induced distributed torque, the regular force is

$$Q_r(t) = \int_0^{L_1+L_2} M_n(x,t)Y_r(x)dx \tag{28}$$

The regular damping is

$$\begin{aligned} C_{Nr} = &\int_0^{L_1+L_2} v_eY_r^2(x)dx = \int_0^{L_1} v_1\left[A_r\left(C_1\sin\frac{\omega_r}{a_1}x + D_1\cos\frac{\omega_r}{a_1}x\right)\right]^2 \\ &+ \int_{L_1}^{L_1+L_2} v_2\left\{A_r\left[C_2\sin\frac{\omega_r}{a_2}(x-L_1) + D_2\cos\frac{\omega_r}{a_2}(x-L_1)\right]\right\}^2 \end{aligned} \tag{29}$$

4.2.4 Canonical equation

The regular coordinate $q_r(t)$ is introduced, and $q_r(t)$ satisfies the following relation:

$$\theta(x,t) = \sum_{r=1}^{\infty} Y_r(x)q_r(t) \tag{30}$$

The canonical equation is

$$\ddot{q}_r + C_{Nr}\cdot\dot{q}_r + \omega_r^2q_r = Q_r(t) \quad r = 1,2,\cdots \tag{31}$$

The initial conditions give us the $q_r|_{t=0} = \dot{q}_r|_{t=0} = 0$.

The fourth-order Runge-Kutta method is used to solve Eq. (31) to solve the torsional vibration equation of the rod string.

5 Simulation Engineering Example

5.1 Essential Parameter

Basic parameters of simulation: carbon fiber rod diameter $D_1 = 19$ mm, carbon fiber rod length $L_1 = 1400$ m, carbon fiber rod density $\rho_1 = 2100\ \mathrm{kg/m^3}$, the shear elastic modulus of the carbon fiber rod $G_1 = 0.653$ GPa, the diameter of the steel rod $D_2 = 22$ mm, the length of the steel rod $L_2 = 600$ m, the density of the steel rod $\rho_2 = 7800$ kg / $\mathrm{m^3}$, the shear elastic modulus of the steel roa $G_2 = 8$ GPa, the inner diameter of the oil pipe $D_\mathrm{r} = 63.5$ mm, the number of strokes $n = 3$, and the axial distributed load $q(x,t)$ and the hanging point load $P(t)$ are shown in Figures 6 and 7. The simplified torsional spring stiffness K_e of the suspension device is shown in Figure 8. The helical buckling of the rod at time t_1 is illustrated in Figure 9. The distributed torque is calculated using this buckling configuration. Since the movement of the sucker rod is periodic, each $t_1 + nT$ moment provides an excitation to the system, as shown in Figure 10.

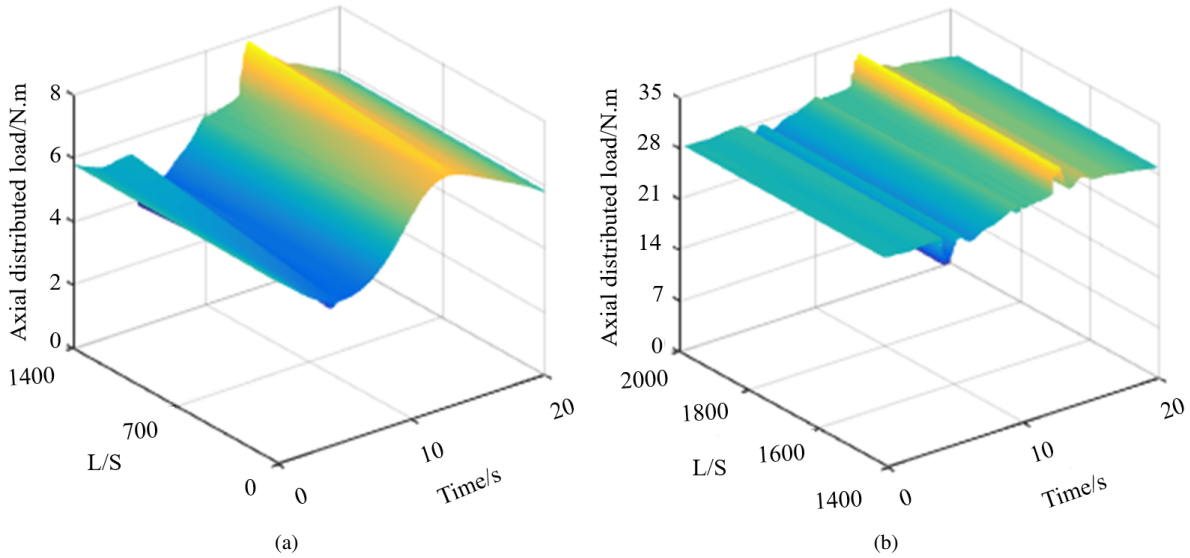

Figure 6. Axial distributed load of carbon fiber and steel hybrid rod. (a) Carbon fiber rod axial distributed load, and (b) axial distributed load on steel rod

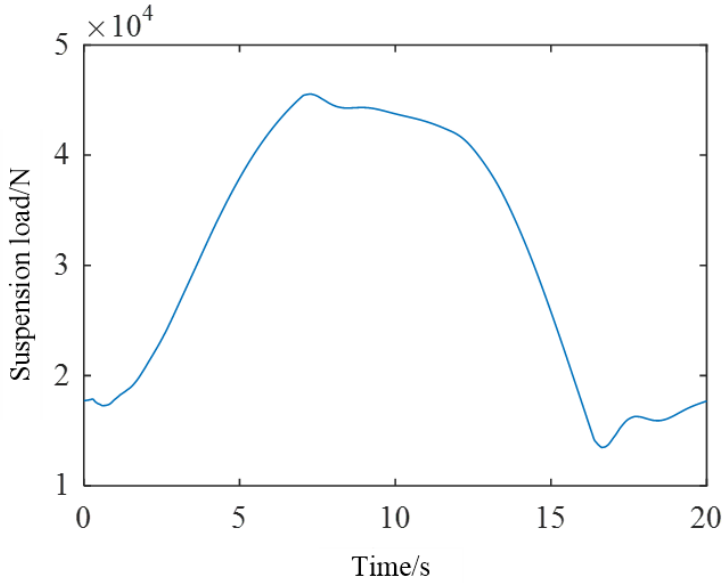

Figure 7. Load at the suspension point

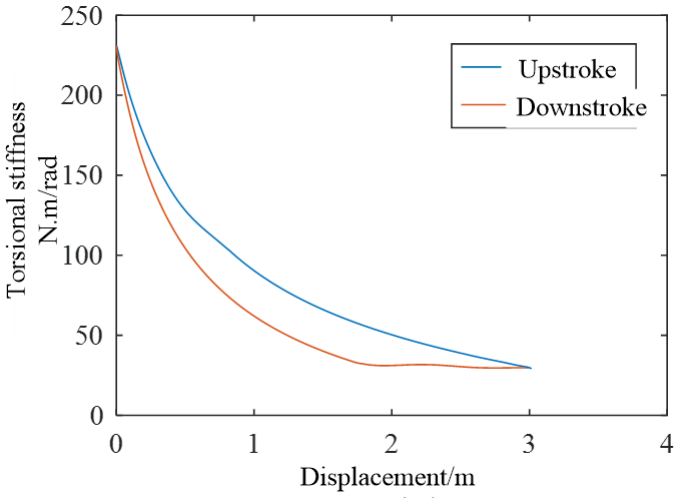

Figure 8. Spring torsional stiffness

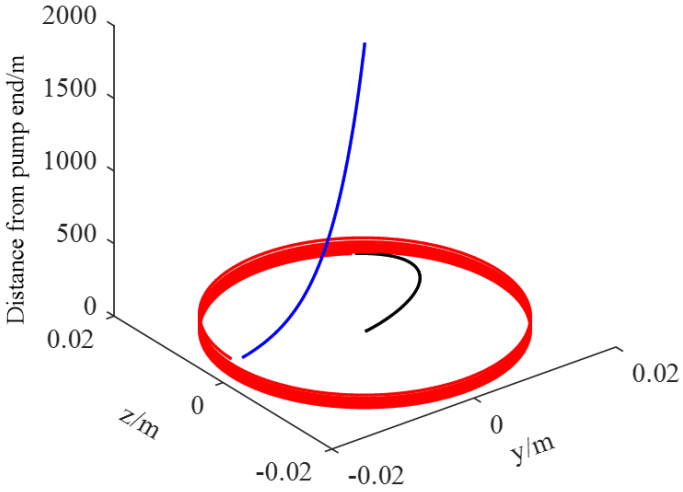

Figure 9. Helical buckling configuration

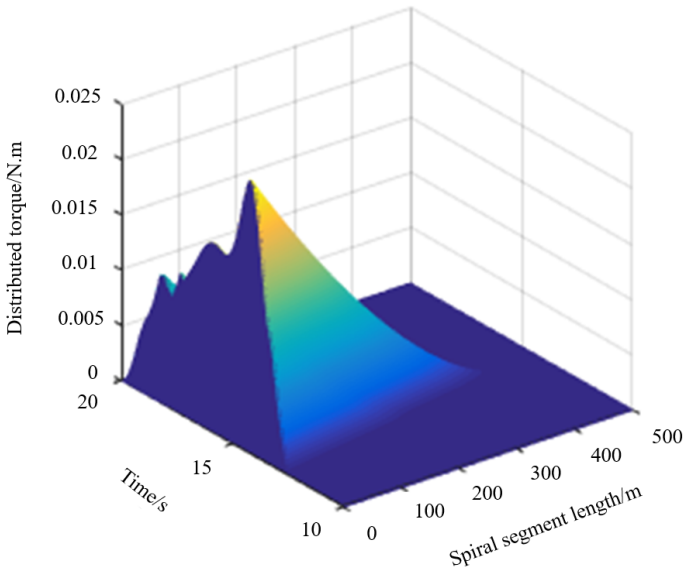

Figure 10. Time of induced distributed torque excitation

5.2 Analysis of Simulation Result

5.2.1 Twist vibration analysis of top rod string

According to the above simulation model, a torsional vibration simulation system of carbon fiber sucker rod string under the torque excitation induced by helical buckling is developed. Figure 11 shows the vibration law of the top rod string in different strokes n in the first 15 cycles.

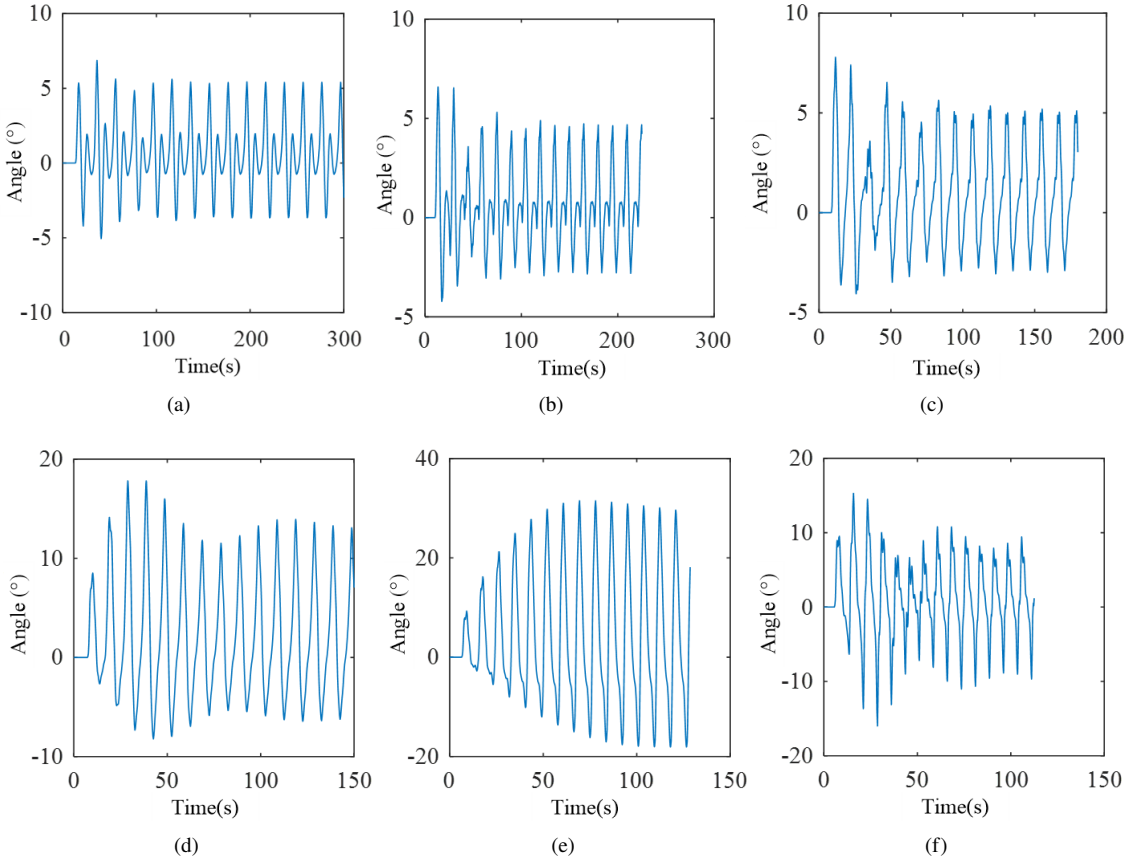

Figure 11. Twist vibration of the top rod string under different strokes. (a) n=3, (b) n=4, (c) n=5, (d) n= 6, (e) n=7, and (f) n= 8

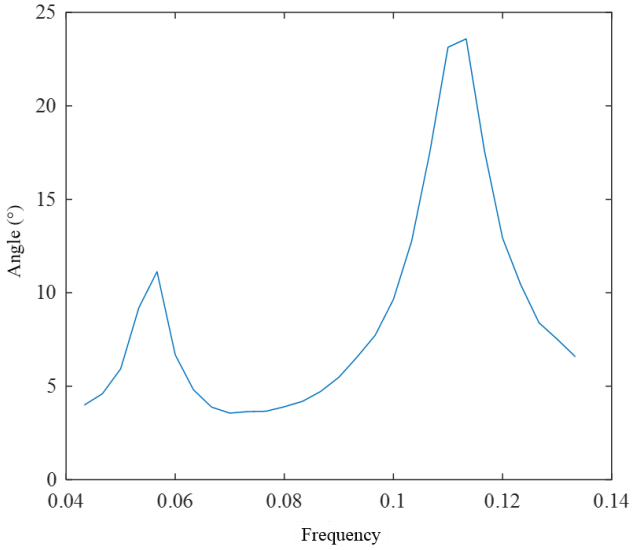

Figure 12. Amplitude-frequency characteristics of the maximum amplitude of vibration at the top of the rod string

As can be seen from Figure 11, with the increase of stroke, the maximum amplitude of the top vibration first increases and then decreases, indicating that resonance is generated. The amplitude-frequency characteristic curve of the maximum amplitude of the top rod string is drawn as shown in Figure 12.

As shown in Figure 12, the torsional vibration system of the carbon fiber sucker rod string has two wave peaks, which are the two resonance points. By averaging the torsional spring stiffness and using the superposition method of vibration modes, the first six natural angular frequencies are calculated, as shown in Table 1. Converting the first-order natural angular frequency to a natural frequency yields 0.1117 Hz, indicating that the second wave peak, or stroke, near 6.7 Hz is the resonance point. The first wave peak occurs because the induced torque is a non-sinusoidal periodic wave, which can be decomposed into a sum of a sine wave of the same frequency and many integer multiples of the frequency. When the integer multiple frequency equals the natural frequency, high-order harmonic resonance occurs.

Table 1. First six order natural angular frequencies

Order	First Order	Second Order	Third Order	Fourth Order	Fifth Order	Sixth Order
Natural angular frequency	0.7020	4.0641	7.9200	11.7895	15.4307	17.0640

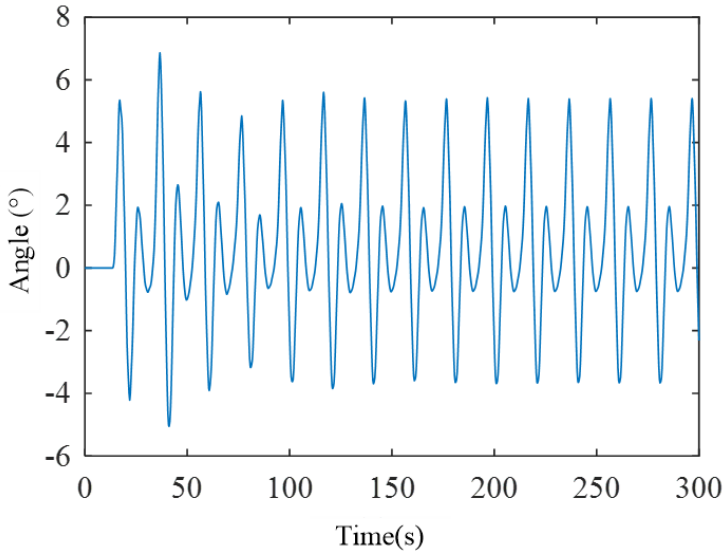

Figure 13. Vibration of the top end of a rod with variable torsional stiffness

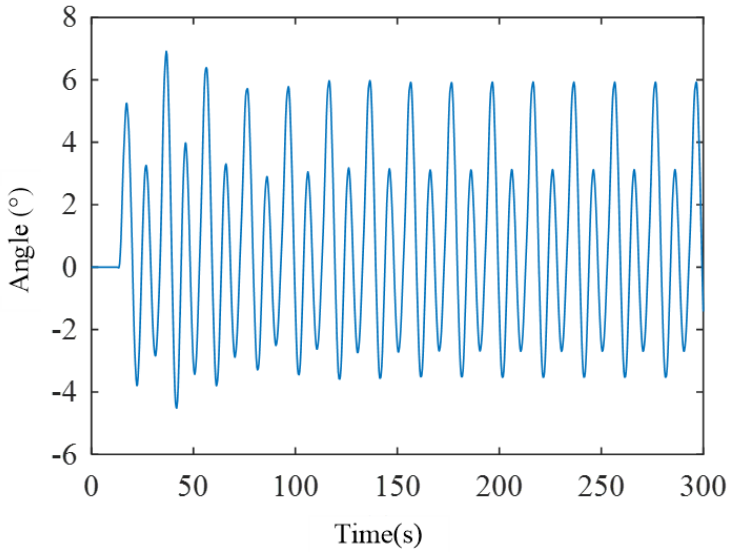

Figure 14. Vibration of the top end of a rod with average torsional stiffness

Figures 13 and 14 show the vibration response curves of the rod string top with variable torsional stiffness and average torsional stiffness. It can be seen that the angular displacement response curves calculated by the finite difference method and the mode superposition method are almost the same. The use of these two calculation methods can verify the correctness of the simulation results in this paper.

5.2.2 Parameter sensitivity analysis

The dynamic characteristics of rod pumping systems are influenced by stroke length, frequency, damping, pump diameter, dynamic liquid level, and well depth. These parameters are of significant interest in the engineering field.

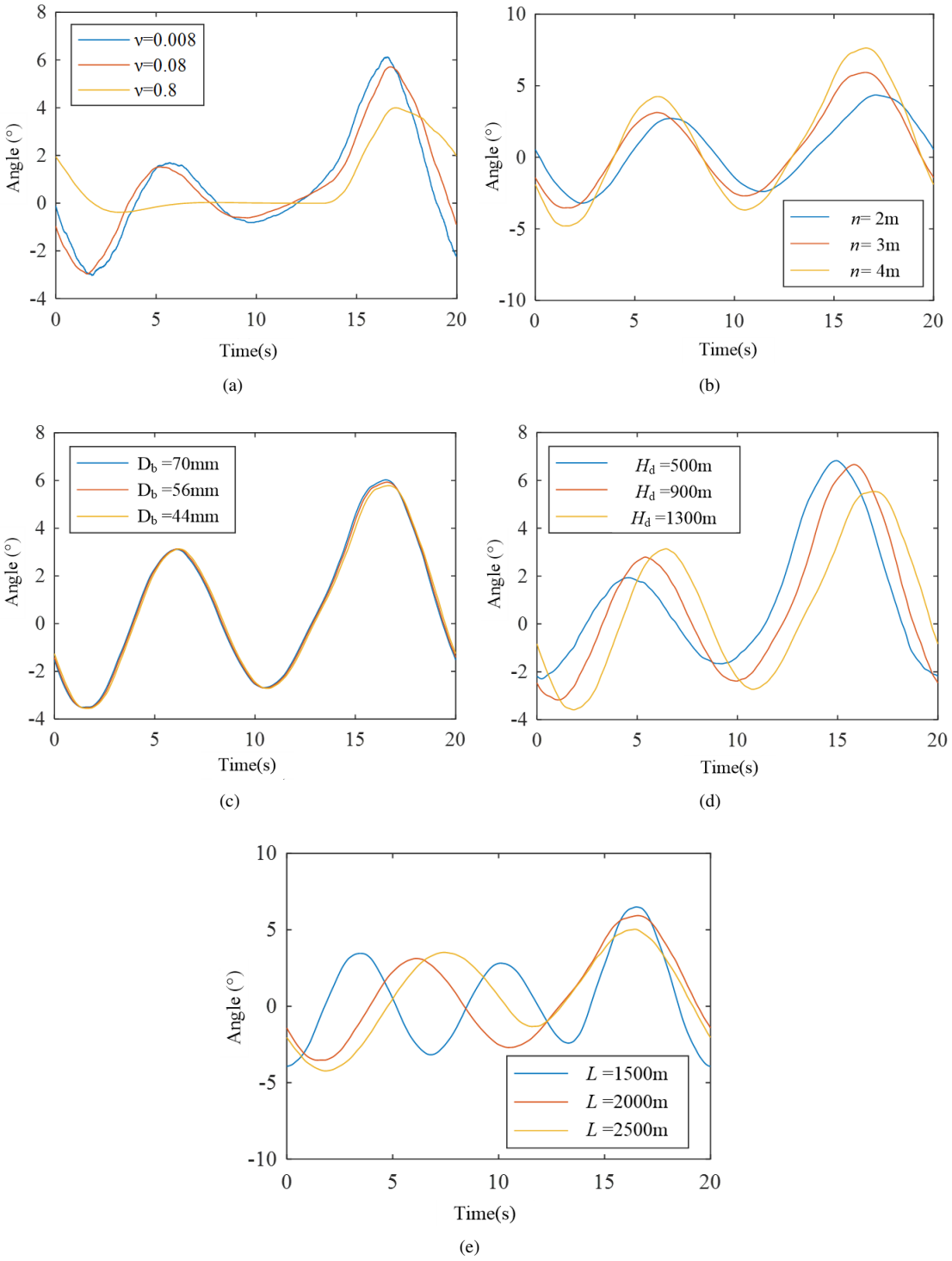

Figure 15. The influence of different parameters on the vibration at the top of the rod string. (a) Damping coefficient v, (b) stroke n, (c) pump diameter D_b, (d) dynamic fluid H_d, and (e) rod length L

Figure 15 illustrates the effects of different parameters on the vibration at the top of the rod string. Figure 15(a) shows that as the damping coefficient increases, the torsional vibration of the rod string decreases. Figure 15(b) indicates that a longer stroke results in a greater amplitude of the stroke pressure under pump end load, leading to a higher induced torque and more intense rod string vibration. Figure 15(c) shows that a smaller pump diameter tends to increase rod string vibration. Figure 15(d) indicates that a lower dynamic liquid level height leads to a greater amplitude of the stroke pressure under pump end load, resulting in a higher induced torque and more intense rod string vibration. Figure 15(e) shows that a longer rod string results in weaker wellhead rod string vibration. The conclusions from Figure 15 are highly consistent with real-world engineering conditions.

5.2.3 Analysis of torsional vibration of rod string excited by bending configuration

In order to obtain the torsional angular displacement along the entire length of the rod, the influence of the suspension device is ignored, and the wellhead is simplified as a fixed end. Two methods are used for simulation. One is without applying the bending configuration excitation, and the other is to apply the bending configuration excitation according to this paper.

1. Analysis of torsion angle of rod string without helical buckling

It can be concluded from Figures 16 and 17 that, under the condition of no bending configuration excitation, the torsional angular displacement difference along the entire well depth is not large, and the torsion situation is relatively uniform along the well depth, slightly larger near the bottom of the well.

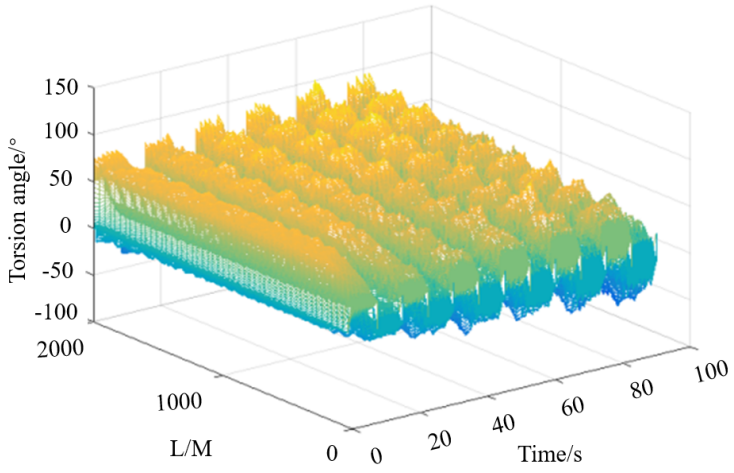

Figure 16. Angle displacement with rod length (bending excitation unapplied)

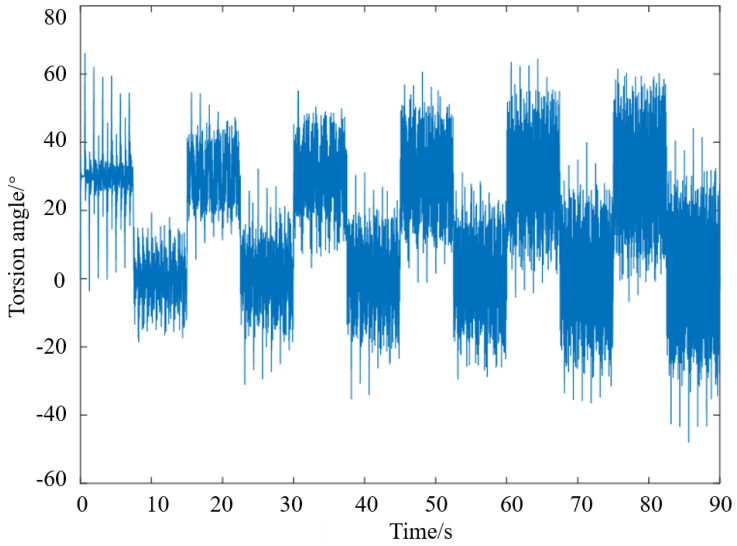

Figure 17. Angle displacement at x=1000 m

2. Analysis of torsion angle of rod string under helical buckling excitation in this paper

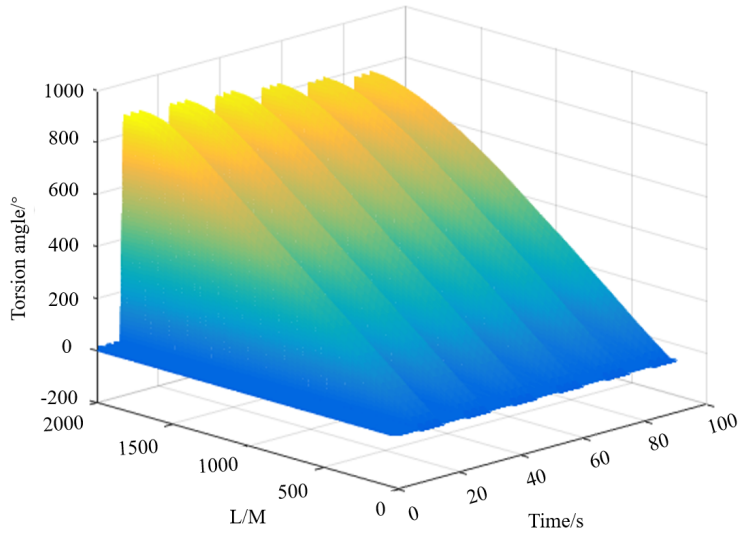

Figure 18. Torsion angle with rod length (bending excitation applied)

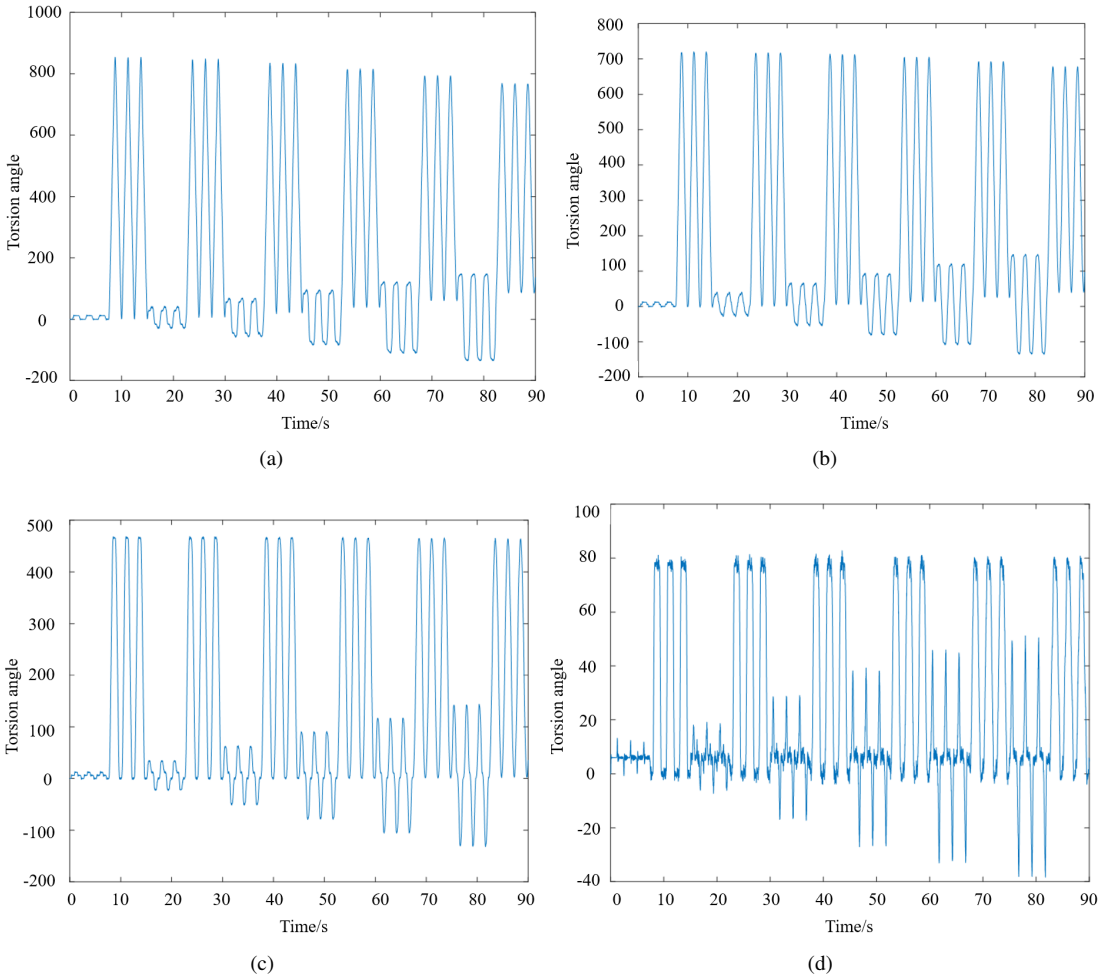

Figure 19. Angle displacement with rod length variation (buckling excitation applied). (a) x=1800 m, (b) x=1500 m, (c) x=1000 m, and (d) x=200 m

From Figures 18 and 19, it is evident that the application of bending configuration excitation significantly affects the torsional vibration of the sucker rod string. The amplitude of the torsional vibration angle displacement increases as the depth of the well approaches the bottom. At the same depth, the angular displacement changes through four

stages over time: In the first stage, the elastic torsional energy of the sucker rod string accumulates, and there is no relative torsional movement; in the second stage, the rod body begins to experience relative torsional movement due to reaching the critical torque, which occupies most of the downstroke; in the third stage, the elastic torsional energy of the sucker rod string is released, and the rod stops experiencing relative torsional movement, typically occurring in the latter part of the downstroke; in the fourth stage, during the upstroke, the bending is minimal, and its effect on torsion can be disregarded. Figures 18 and 19 demonstrate that helical buckling has a significant impact on the overall torsional vibration of the sucker rod string, with the torsional effect primarily concentrated in the middle and lower parts of the well. This conclusion aligns with the analysis of the torsional process described in the study [12], indicating consistency between the simulation results and previous practical experience, and can serve as an experimental validation for this study.

6 Conclusions

(1) The mechanical model and the mathematical model of torsional vibration of carbon fiber sucker rod string with top torsion spring constraint are established, and the response is calculated by the finite difference method and the mode superposition method.

(2) Through the analysis of the torsional vibration law of carbon fiber sucker rod string, it can be concluded that with the increase of stroke, the torsional vibration first increases and then decreases, so as to avoid the generation of resonance; damping coefficient, stroke, pump diameter, dynamic liquid level, and rod length have a great influence on the torsional vibration of the rod string.

(3) Through the simulation of torsional vibration by helical buckling, it is concluded that helical buckling has a significant influence on the overall torsional vibration of the rod string, and the torsion is mainly concentrated in the middle and lower part of the well depth.

(4) The torsional vibration simulation model of the carbon fiber sucker rod string under the torque excitation induced by helical buckling can further analyze the longitudinal splitting mechanism of the carbon fiber sucker rod, and provide a theoretical basis for improving the working life and design of the carbon fiber sucker rod string.

Funding

This work is funded by Science Research Project of Hebei Education Department of China (Grant No.: ZC2023164) and Science and Technology Key Project of Hebei University of Environmental Engineering (Grant No.: 2020ZRZD01).

Data Availability

The data used to support the research findings are available from the corresponding author upon request.

Conflicts of Interest

The authors declare no conflict of interest.

References

[1] C. Carpenter, "Fiber-reinforced thermoplastic sucker rods provide artificial lift efficiencies," *J. Pet. Technol.*, vol. 76, no. 10, pp. 85–87, 2024. https://doi.org/10.2118/1024-0085-jpt

[2] J. Saponja, C. Coyes, and M. Conner, "Fiber reinforced thermoplastic (FRTP) sucker rods providing high strength light weight low cost and environmentally responsible artificial lift efficiencies," in *International Petroleum Technology Conference, Dhahran, Saudi Arabia*, 2024. https://doi.org/10.2523/iptc-23949-ms

[3] H. Krechkovska, B. Bakun, I. Kopey, and O. Student, "Feature of fatigue fracture of the composite sucker rod," *Procedia Struct. Integrity*, vol. 59, pp. 292–298, 2024. https://doi.org/10.1016/j.prostr.2024.04.042

[4] K. Naito, "Interfacial mechanical properties of carbon/glass hybrid thermoplastic epoxy composite rods," *Compos. Struct.*, vol. 257, p. 113129, 2021. https://doi.org/10.1016/j.compstruct.2020.113129

[5] H. Krechkovska, B. Kopey, B. Bakun, and I. Kopey, "Pecularities of fatigue cracks growth in steel and composite sucker rods," *Procedia Struct. Integrity*, vol. 42, pp. 1406–1413, 2022. https://doi.org/10.1016/j.prostr.2022.12.179

[6] R. Albishini, "Design of a novel protector for sucker rod pumps using wire rope," mastersthesis, Montanuniversität Leoben, 2019. https://doi.org/10.34901/MUL.PUB.2024.195

[7] P. Eisner, C. Langbauer, and R. Fruhwirth, "Sucker rod pump downhole dynamometer card determination based on a novel finite element method," *Liq., Gas. Energy Resour.*, 2021. https://doi.org/10.21595/lger.2021.22004

[8] X. Sun, S. Dong, H. Wang, W. Li, and L. Sun, "Comparison of multistage simulation models of entire sucker rod with spatial buckling in tubing," *J. Jilin Univ. Eng. Technol. Ed.*, vol. 48, no. 4, pp. 1124–1132, 2018. https://doi.org/10.13229/j.cnki.jdxbgxb20170512

[9] C. Eritici, "Compressive forces causing rod buckling in sucker rod pumps and using sinker bars to prevent buckling," *Univ. Texas Lib.*, 2016.

[10] Q. B. Yue, J. B. Liu, and R. Z. Dong, "The research of post-buckling about slender rod string in wellbore based on energy method and experiment," *J. Pet. Sci. Eng.*, vol. 156, pp. 732–739, 2017. https://doi.org/10.1016/j.petrol.2017.06.046

[11] R. F. Mitchell, "The twist and shear of helically buckled pipe," *SPE Drill. Completion*, vol. 19, no. 1, pp. 20–28, 2004. https://doi.org/10.2118/87894-pa

[12] X. Zhu, Q. Liu, F. Li, F. Liu, and H. Dong, "Discuss of contribution factors of sucker rod torsional vibration," *J. Southwest Pet. Univ. Sci. Technol. Ed.*, vol. 2003, no. 5, pp. 78–80+92, 2003. https://doi.org/10.3863/j.issn.1000-2634.2003.05.22

[13] A. Zdvizhkov, S. Miska, and R. Mitchell, "Measurement and analysis of induced torsion in helically buckled tubing," *SPE Drill. Completion*, vol. 24, no. 2, pp. 266–275, 2009. https://doi.org/10.2118/92274-pa

[14] J. Chen, Y. Qi, X. Liu, and C. Liu, "Study on 3-D vibrations of sucker rod string based on the elastic body vibration theory," *Pet. Min. Mach.*, vol. 38, no. 2, pp. 15–19, 2009.

[15] A. A. Isaev, M. M. O. Aliev, A. N. Drozdov, Y. A. Gorbyleva, and K. S. Nurgalieva, "Improving the efficiency of curved wells' operation by means of progressive cavity pumps," *Energies*, vol. 15, no. 12, p. 4259, 2022. https://doi.org/10.3390/en15124259

[16] S. Toumi and R. Mlayeh, "Control strategies for mitigating torsional and axial vibrations in rotary oilwell drilling systems," *IMA J. Appl. Math.*, vol. 89, no. 4, pp. 705–724, 2024. https://doi.org/10.1093/imamat/hxae030

[17] H. Wang, X. Sun, F. Li, W. Li, S. Xin, C. Wang, and D. Li, "Simulation study of sucker rod string on longitudinal, transverse and torsional coupling vibration in directional wells," *J. Vib. Eng.*, vol. 37, no. 11, pp. 1936–1949, 2024. https://doi.org/10.16385/j.cnki.issn.1004-4523.2024.11.014

[18] J. Rodríguez and J. Merodio, "Helical buckling and postbuckling of pre-stressed cylindrical tubes under finite torsion," *Finite Elem. Anal. Des.*, vol. 112, pp. 1–10, 2016. https://doi.org/10.1016/j.finel.2015.12.003

[19] N. K. Jha, S. Moradalizadeh, J. Reinoso, H. Topol, and J. Merodio, "On the helical buckling of anisotropic tubes with application to arteries," *Mech. Res. Commun.*, vol. 128, p. 104067, 2023. https://doi.org/10.1016/j.mechrescom.2023.104067

[20] V. Balbi and P. Ciarletta, "Helical buckling of thick-walled, pre-stressed, cylindrical tubes under a finite torsion," *Math. Mech. Solids*, vol. 20, no. 6, pp. 625–642, 2015. https://doi.org/10.1177/1081286514550570

[21] H. Wang, S. Dong, Y. Zhang, S. Wang, and X. Sun, "Coupling simulation of the pressure in pump and the longitudinal vibration of sucker rod string based on gas-liquid separation," *Acta Pet. Sin.*, vol. 44, no. 2, pp. 394–404, 2023. https://doi.org/10.7623/syxb202302014

[22] X. Sun, S. Dong, M. Liu, and J. Zhang, "The simulation model of sucker rod string transverse vibration under the space buckling deformation excitation and rod-tubing eccentric wear in vertical wells," *J. Vibroeng.*, vol. 20, no. 1, pp. 283–299, 2018. https://doi.org/10.21595/jve.2017.19138